Int. J. Heat Mass Transfer. Vol. 36, No. 15, pp. 3859–3868, 1993
Printed in Great Britain

0017–9310/93 $6.00 + 0.00
Pergamon Press Ltd

Saturated pool nucleate boiling mechanisms at high heat fluxes

KEMAL O. PASAMEHMETOGLU, PADMANABHA R. CHAPPIDI, CETIN UNAL and RALPH A. NELSON

Los Alamos National Laboratory, Nuclear Technology and Engineering Division, Engineering and Safety Analysis Group, Los Alamos, NM 87545, U.S.A.

(*Received* 28 *January* 1992 *and in final form* 9 *September* 1992)

Abstract—A new model has been developed where the coupled transient two-dimensional conduction equation is solved for the heater and the liquid macrolayer, while allowing for the time-wise thinning of the macrolayer. The major conclusions are: (1) dominant evaporation occurs at the liquid–vapor–solid contact point (triple point) and is required to match boiling curve behavior quantitatively; (2) evaporation at the stem interface and bubble–macrolayer interface is negligible (except near critical heat flux); and (3) the results are sensitive to closure relationships, especially to the active site-density correlation.

INTRODUCTION

NUCLEATE boiling has long been recognized as a highly efficient heat-transfer mechanism favored in many industrial applications. Despite its widespread use and numerous studies dealing with various aspects of the process, understanding the mechanisms that influence nucleate boiling and their interactions remains one of the most challenging problems of heat transfer. Until recently, there have been very few detailed mechanistic models aimed at nucleate boiling modeling.

The present paper has two objectives. The first, which will be done in this introductory section, is to briefly bring into perspective recent modeling work of the high heat-flux, saturated-pool, nucleate boiling process. The second objective is to use numerical simulation to address issues that we feel are fundamental to this boiling region. This second objective will be undertaken in the remainder of the paper.

The high-flux, nucleate boiling region, or the vapor mushroom region, was defined in the pioneering study of Gaertner [1]. Various investigators postulated that this region is characterized by the formation of a liquid layer (macrolayer) underneath a growing mushroom-shaped bubble (see Fig. 1). Vaporization of the macrolayer feeds the mushroom as it grows and departs from the surface.

Considerable evidence in the literature confirms the existence of the macrolayer under a growing mushroom. In addition to the visual observations (see Gaertner [1]), Iida and Kobayasi [2] and Bhat *et al.* [3] confirmed the existence of a liquid-rich layer near the heated surface through measurements of void fraction as a function of position above the heated surface using a conductance probe. For the heat fluxes of interest, the average experimentally measured macrolayer thickness ranges from 50 to 500 μm. Line-averaged void fraction measurements made using gamma densitometers [4] confirm macrolayer existence but do not detect the liquid layer in all cases because the minimum distance of the beam from the wall was 300 μm. Indirect evidence of the existence of the macrolayer is also provided by Yu and Mesler [5], who measured surface temperature fluctuations at high heat fluxes.

What might be called 'the ultimate application of the macrolayer concept' has been the use of its existence to explain the occurrence of the critical heat flux (CHF). Katto and his co-workers [6–8] have contributed considerably in defining and analyzing this boiling mechanism leading to the 'multi-step' CHF

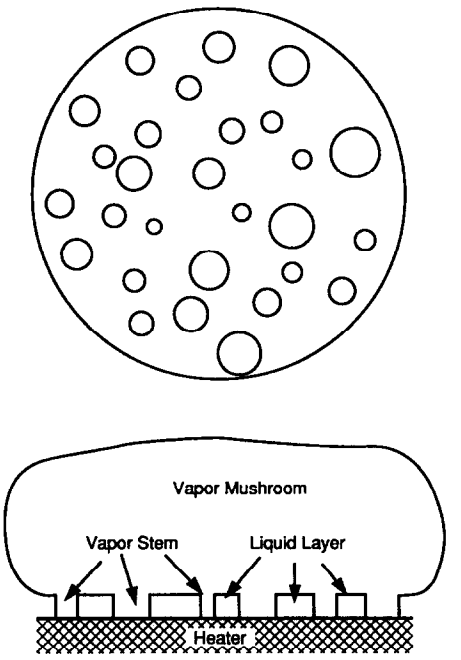

FIG. 1. Schematic of the top and side views of a vapor mushroom over a heated surface.

NOMENCLATURE

A_v	heater area covered by stems [m^2]
A_w	total heater area [m^2]
C	specific heat [J kg^{-1} °C^{-1}]
g	gravitational acceleration [m s^{-2}]
h_c	convective heat-transfer coefficient [W m^{-2} °C^{-1}]
h_e	evaporation heat-transfer coefficient [W m^{-2} °C^{-1}]
h_{fg}	latent heat of vaporization [J kg^{-1}]
H	heater thickness [m]
k	thermal conductivity [W m^{-1} °C^{-1}]
$m_{e,TP}$	triple-point evaporation rate [kg m^{-1} °C^{-1} s^{-1}]
N	number of active sites (dimensionless)
q_e	equivalent heat flux [W m^{-2}]
q_0	boundary heat flux [W m^{-2}]
Q_0	internal heat-generation rate [W m^{-3}]
r	radial coordinate [m]
R_h	heater radius per stem [m]
R_s	stem radius [m]
t	time [s]
T	temperature [°C]
T_c	contact temperature [°C]
T_0	boundary temperature [°C]
T_{sat}	saturation temperature [°C]
T_{TP}	triple-point temperature [°C]
T_w	wall temperature [°C]
z	axial coordinate [m].

Greek symbols

δ	macrolayer thickness [m]
δ_0	initial macrolayer thickness [m]
Δr	radial nodal spacing [m]
Δz_m	axial nodal spacing in the macrolayer [m]
Δz_v	axial nodal spacing between the last two top nodes in the macrolayer [m]
$\Delta\delta$	amount of macrolayer evaporated [m]
ρ	density [kg m^{-3}]
σ	surface tension [N m^{-1}]
τ_d	bubble departure time [s].

Subscripts

f	liquid
g	vapor
h	heater.

model [8]. Experimental and analytical transient CHF studies [9, 10] also demonstrate the importance of this concept.

Thus, although the existence of the macrolayer is accepted, how it evaporates to supply the mushroom bubble and some of its basic characteristics are still under serious debate. The literature contains several detailed phenomenological models aimed at analyzing the boiling curve behavior of this boiling regime. We provided an extensive literature review on the subject elsewhere [11]. Generally, these models may be classified in terms of their emphasis on the dominant phenomena. The more significant aspect of several of the various models may be classified as follows.

Transient one-dimensional (1D) models

Studies aimed at detailed 1D modeling of the macrolayer evaporation phenomenon are provided by authors [3, 12–14] who concluded that the conduction across the macrolayer and evaporation from the top interface of the macrolayer was the dominant mechanism. This conclusion was strongly questioned by Chyu [15]. However, Chyu's [15] conclusion was not backed by detailed analysis and was based mostly on qualitative arguments. In a sense, Chyu's [15] model may be considered to be 1D also, as it is mainly concerned with 1D conduction across the microlayer under the vapor stem. This microlayer concept might be thought of as being similar to that associated with discrete bubbles. However, the implications of such localized evaporation on the wall temperature and the resulting nonuniformities were not quantified by Chyu [15].

The study of Pan *et al.* [16] may also be classified under 1D models. However, the authors assumed that the nucleate-boiling near the vapor stem was the dominant evaporation mechanism, as opposed to the conclusions of refs. [3, 12–14].

In the study of Jairajpuri and Saini [14], the constant wall superheat assumption of previous 1D models was replaced by a constant wall heat-flux assumption, allowing for time-wise variations in wall superheat and macrolayer thickness to occur. However, while the authors showed the correct heat fluxes that were obtained, time-averaged wall temperature results were not shown.

The major shortcomings of the 1D models are that a priori assumptions have to be made on the dominant evaporation mechanisms and on the elimination of wall superheat spatial variations in the tangential direction. While the validity of the uniform wall temperature assumption might be argued for isothermal heater materials such as copper, the majority of common engineering materials are not isothermal. The temporal constant wall temperature assumption frequently employed also contradicts the temperature fluctuations observed by Yu and Mesler [5].

Steady-state, two-dimensional (2D) models

The studies of Dhir and Liaw [17] and Pan and Lin [18] investigate some 2D aspects of the problem. In both studies, the thermal behavior of the macrolayer

is treated as steady-state and macrolayer thinning is ignored. The study of Dhir and Liaw [17] does not recognize the existence of the macrolayer. Their analysis implies that the thermal boundary layer is much smaller than the liquid layer thickness; consequently, the macrolayer thickness is irrelevant to the analysis. Within their own database, Dhir and Liaw [17] achieved reasonable success in modeling their high-flux boiling and CHF data. Further details of this model and its comparison to 'macrolayer models' are provided elsewhere [11]. Pan and Lin [18] attempted to include flow effects within the macrolayer in the analysis. They postulated that both Marangoni flow and interfacial shear-induced flow resulting from vapor flows out of the stem result in an enhancement of the effective liquid thermal conductivity.

As with 1D models, the major shortcoming of these studies is the uniform and constant surface-temperature assumption.

Issues. We believe the major issues arising from previous studies are as follows:

(a) The modeling efforts are predominantly either transient 1D or steady-state two-dimensional (2D). Steady-state models imply that liquid resupply does not disturb the thermal boundary layer profile within the macrolayer. Transient models imply that the thermal profile is disturbed by the liquid resupply, and we consider its re-establishment to be important. Frequently hidden within the transient models is the question of the initial temperature of the resupplied liquid.

(b) Macrolayer thinning is generally not considered.

(c) A constant and uniform temperature heater, surface-boundary condition was used in most of the previous studies.

(d) Contact angle effects have been studied in few of the models. While we believe Dhir and Liaw's [17] model does have several significant limitations, their investigation of this effect is a meaningful undertaking.

The present study is aimed at a more detailed analysis of the macrolayer evaporation mechanism using a transient 2D model to include both the macrolayer and the heater. The model used in the current study is described in the following section. Results obtained using the model and conclusions are then presented.

MODEL DESCRIPTION

In this study, we modeled the problem as a transient 2D conduction-dominated problem considering both the macrolayer and the heater. Thinning of the liquid macrolayer is included. Such an approach allows us to address the following points: (1) the uniform and constant wall-temperature solution may be relaxed; (2) the influence of both heater materials and their thickness can be studied; (3) the effect of the heating method may be investigated; and (4) parametric studies with the transient 2D model may provide clues to the 3D behavior of the problem. The present paper mainly emphasizes the first point. The second point is also discussed briefly within the paper.

Figure 2 shows the physical model. The most significant feature of this vapor stem macrolayer model is the introduction of a liquid–vapor–solid, contact-point evaporation phenomena, also called the microlayer evaporation hypothesis, in the macrolayer evaporation model. (The liquid–vapor–solid contact-point/circle will be called the triple point.) This visualization of the microlayer at high heat fluxes differs from earlier propositions [15]. Chyu's [15] microlayer hypothesis shows a continuous layer of liquid film underneath the vapor stem. Rather, we believe that such continuous existence is unlikely and that the microlayer has a dry spot at the center of the stem as experimentally observed by Kirby and Westwater [19] and Van Ouwerkerk [20]. For a moderately wetting fluid such as water, evaporation from the microlayer (whose location may well be dynamic during a bubble's lifetime) is a highly efficient mechanism, and the liquid macrolayer may evaporate through microlayer consumption.

The scale of the microlayer region is expected to be much smaller than the scale of the macrolayer; our analysis (to be shown later) indicates that the stem's liquid–vapor interface, by itself, does not provide an efficient evaporation mechanism. This leads us to conjecture that the triple-point phenomena representing the microlayer evaporation must occur rather close to the heater surface.

Modeling the details of the microlayer at high heat fluxes would require a true characterization of the curved liquid–vapor interface near the triple-point. For now, we note that the microlayer evaporation effect is represented in the model in a lumped sense. A triple-point mass evaporation coefficient, $m_{e,TP}$ (kg s^{-1} m^{-1} K^{-1}), represents the mass of liquid evaporated per unit time per unit perimeter of the vapor stem per degree wall superheat of the triple point. We expect the microlayer shape and scale to be influenced by several factors, such as the contact angle between the fluid and the heater surface. For example, with a highly wetting fluid, the scale of the microlayer may be thinner than for a moderately wetting fluid. The evaporation rate at the triple point will depend upon the scale and shape of the microlayer. To cover a wide range of contact angles and surface characteristics (representing different fluid–heater surface combinations and conditions), a correlation of the triple-point, mass-evaporation coefficient with respect to the contact angle would be required. In the current work, the only data considered is for the saturated water–copper surface combination. If the current model is used to make predictions for other sets of data with different fluids, the triple-point evaporation coefficient would have to be revised.

Governing equations

The present 2D model consists of the solution of the transient conduction equation within a region

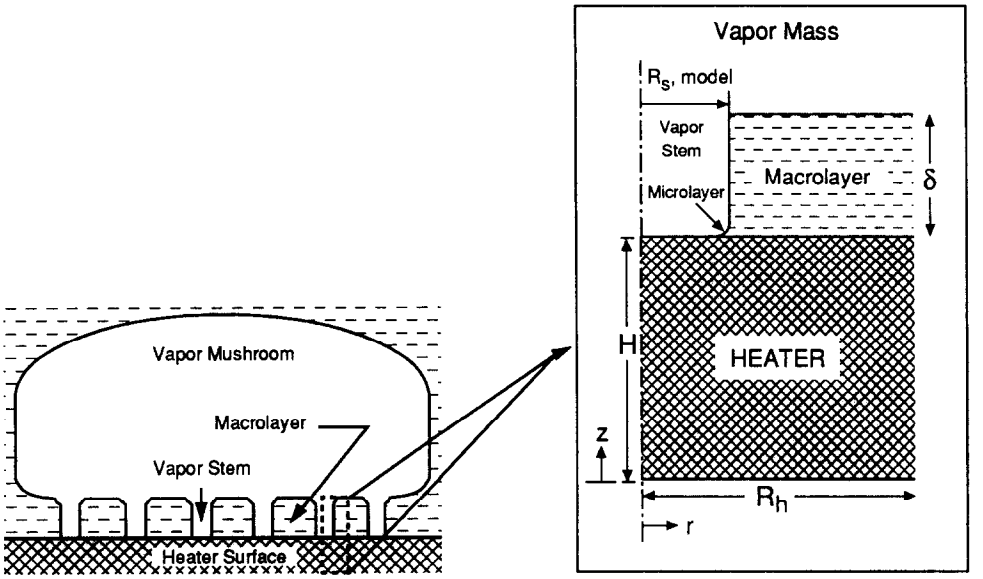

FIG. 2. Schematic of a 2D single stem model.

including both the heater and the macrolayer. For the heater, the 2D conduction equation in cylindrical coordinates is

$$\rho_h C_h \frac{\partial T}{\partial t} = k_h\left(\frac{\partial^2 T}{\partial r^2} + \frac{1}{r}\frac{\partial T}{\partial r} + \frac{\partial^2 T}{\partial z^2}\right) + LP \times Q_0 \quad (1)$$

where LP represents the problem type and is equal to 1 for internal heat generation and 0 for constant heat flux or temperature boundary condition at the bottom of the heater. Neglecting convective effects, the governing equation within the liquid macrolayer, becomes

$$\rho_f C_f \frac{\partial T}{\partial t} = k_f\left(\frac{\partial^2 T}{\partial r^2} + \frac{1}{r}\frac{\partial T}{\partial r} + \frac{\partial^2 T}{\partial z^2}\right). \quad (2)$$

Boundary conditions

The boundary conditions for the heater at $z = 0$ and for all r's are

$$-k_h \frac{\partial T}{\partial z} = q_0 \quad \text{or} \quad T = T_0 \quad \text{for} \quad LP = 0,$$

$$\text{and} \quad \frac{\partial T}{\partial z} = 0 \quad \text{for} \quad LP = 1.$$

The boundary conditions at $r = 0$ and R_h, for all z, come from the symmetry condition given by $\partial T/\partial r = 0$ at $r = 0$, and $r = R_h$ for all z between 0 and H. The validity of these boundary conditions can be inferred from the final transient solution.

Underneath the vapor stem ($r < R_s$ and $z = H$), the boundary condition becomes

$$-k_h \frac{\partial T}{\partial z} = h_c(T - T_{sat})$$

where h_c is the convective heat-transfer coefficient to vapor. For the studies reported in this paper, h_c is set to zero.

Finally, at the heater upper surface where the liquid macrolayer and the heater are in contact ($R_s \leqslant r \leqslant R_h$), the boundary conditions are as follows:

$$(T)_{z=H^-} = (T)_{z=H^+}$$

$$\text{and} \quad k_h\left(\frac{\partial T}{\partial z}\right)_{z=H^-} = k_f\left(\frac{\partial T}{\partial z}\right)_{z=H^+}.$$

Within this formulation, the triple-point becomes a discontinuity point. The evaporation of the microlayer, which penetrates under the vapor stem, is represented by including an evaporation coefficient, h_e. The penetration length of this liquid is unknown; however, we assumed that its evaporation takes place within a small surface area centered around $z = H$ and $r = R_s$, so that

$$-k_h\left(\frac{\partial T}{\partial z}\right)_{z=H^-,\,r=R_s} = h_e[(T)_{z=H^+,\,r=R_s} - T_{sat}].$$

At the macrolayer–vapor–mass and macrolayer–stem interfaces, the vapor temperature is assumed to be the saturation temperature. A static force balance around the circumference of the stems indicates that, for the stem diameter values reported in the literature, the effect of surface tension is negligble, and the vapor pressure inside the stem may be approximated by the liquid pressure. Thus, no vapor superheat is required from pressure considerations. However, vapor superheat may result from heat transfer to vapor and interfacial resistance. Such effects are initially neglected in the present study, resulting in the following macrolayer interface boundary condition:

$$T = T_{sat} \quad \text{at} \quad z = H+\delta \quad \text{and} \quad R_s \leqslant r \leqslant R_h$$

$$\text{and} \quad T = T_{sat} \quad \text{at} \quad r = R_s \quad \text{and} \quad H < z \leqslant H+\delta.$$

These boundary conditions allow the maximum evaporation possible from the macrolayer–vapor interfaces.

As discussed before, the macrolayer boundary condition at $r = R_h$ can be found from symmetry, as $\partial T/\partial t = 0$ at $r = R_h$ and $H \leqslant z \leqslant H+\delta$. This implies that a 1D solution would apply when $r \geqslant R_h$ until the next stem is approached.

Initial conditions

For each point on the steady-state boiling curve, a transient solution involving the growth and departure of vapor mushrooms and heater–macrolayer thermal response is desired.

To start the calculation (the first bubble period), a temperature distribution corresponding to the 1D steady-state solution is assumed for the heater temperature profile. For subsequent bubbles, the internal heater temperature distribution at the beginning of a bubble's life is the same as the temperature distribution at the departure of the previous bubble. After a certain number of bubble lifetimes (periods), the effect of the initial guess for the heater temperature distribution vanishes, and the heater solution becomes stationary with respect to each bubble lifetime.

The photographs of Katto and Yokoya [7] show that the delay time for mushroom bubble formation is much smaller than the bubble hovering period for high heat-flux boiling. On this basis, we assume no delay time is associated with the establishment of the liquid macrolayer. Thus, at the time of bubble departure and birth of the new bubble, we assume that fresh saturated liquid wets the surface. The initial condition for the macrolayer becomes $T = T_{sat}$ and is used at the beginning of every bubble's life. This assumption allows the maximum effect of liquid resupply and also agrees with the results of Yu and Mesler [5]. As noted in the introduction, the steady-state solutions provide the other extreme where the incoming liquid does not disturb the established thermal boundary layer.

After bubble departure and contact with fresh liquid, the resulting macrolayer–heater interfacial temperature is calculated through the instantaneous contact temperature relationship for two semi-infinite solids and is given by

$$T_c - T_{sat} = \frac{T_w - T_{sat}}{1+\sqrt{\dfrac{(k_f C_f \rho_f)}{(k_h C_h \rho_h)}}}. \tag{3}$$

Yu and Mesler [5] showed that the instantaneous contact temperature of the heated wall with saturated liquid is able to successfully explain the sudden temperature drop after bubble departure.

Macrolayer and triple-point evaporation

Except at very high heat fluxes just before CHF, little is known about whether vapor-stem growth or vertical macrolayer thinning results from the evaporation. The direction of dominant interfacial motion will most likely be determined by which macrolayer interface dominates evaporation. As noted in the Introduction, the dominant evaporative effect is still hotly debated. Because of this lack of knowledge and that it is easier to model in this first attempt, we assume only the macrolayer thickness changes as a function of time because of evaporation. Thus, the vapor stem diameter R_s for each point on the boiling curve is assumed constant during bubble growth. As long as we limit ourselves to high heat fluxes that do not approach total evaporation of the macrolayer evaporation, this assumption should not significantly affect the results.

With this assumption in mind, macrolayer thinning is formulated as

$$\pi\rho_f h_{fg}(R_h^2 - R_s^2)\frac{d\delta}{dt} = \left[2\pi k_f \int_{R_s}^{R_h}\left(\frac{\partial T}{\partial z}\right)_{z=H+\delta} r\,dr\right] - \left[2\pi R_s k_f \int_H^{H+\delta}\left(\frac{\partial T}{\partial r}\right)_{r=R_s} dz\right] - \left\{2\pi \int_{R_s-\Delta R_s/2}^{R_s+\Delta R_s/2} h_e[T(H, R_s, t) - T_{sat}] r\,dr\right\}. \tag{4}$$

The first, second, and third terms on the right-hand side (RHS) represent the evaporation along the macrolayer–vapor mass interface, macrolayer–stem interface, and the triple-point, respectively. After each bubble departure, the initial macrolayer thickness becomes δ_0. For any constant h_e, the solution becomes node size-dependent (depending on Δr). To circumvent this problem, we defined a triple-point, evaporation-rate parameter as $m_{e,TP} \equiv h_e \Delta r/h_{fg}$. This evaporation rate is defined per unit stem perimeter and per unit triple-point superheat. It is the adjustable parameter in the calculations. Thus, the third term on the RHS of equation (4) can be rewritten as $m_{e,TP} h_{fg} 2\pi R_s (T_{TP} - T_{sat})$.

Physically, $m_{e,TP}$ models the evaporation of the microlayer, shown in Fig. 2. It lumps together a number of unknown interactions and phenomena including contact angle and enhanced thermal conductivity effects near the triple point. The use of this model is valid as long as the size of the microlayer penetration under the stem is much smaller than Δr.

Closure relationships used in the model

The model requires various closure relationships to calculate the vapor mass hovering period τ_d and the geometric parameters, i.e. the initial macrolayer thickness δ_0, the stem radius R_s, and the heater radius per stem R_h. The hovering period is estimated from the idealized bubble solution of Katto and Yokoya [7], given by

$$\tau_d = \left(\frac{3}{4\pi}\right)^{1/5}\left[\frac{4(\rho_f+\rho_g)}{g(\rho_f-\rho_g)}\right]^{3/5}\left(\frac{A_w q}{\rho_g h_{fg}}\right)^{1/5}. \quad (5)$$

In equation (5), the surface heat flux q is set to the time- and area-averaged, steady-state heat flux q_e. For simplicity, this study assumes a constant volumetric growth rate based on our earlier study [21], which showed that the transient effects are minimum in calculating the hovering period. However, this approach is only valid for the largest wake-free bubbles defined by Katto and Yokoya [7]. This later assumption could be relaxed in the future to consider multiple bubble periods.

The initial macrolayer thickness δ_0 is estimated using the Helmholtz instability model [8] that yields

$$\delta_0 = \frac{\pi}{2}\sigma\left(\frac{\rho_f+\rho_g}{\rho_f\rho_g}\right)\left(\frac{A_v}{A_w}\right)^2\left(\frac{\rho_g h_{fg}}{q}\right)^2. \quad (6)$$

For the area ratio, we used the empirical equation that we developed based upon the thickness data of Bhat *et al.* [3], which is given by ref. [22]

$$\frac{A_v}{A_w} = 6.206\times 10^{-4} q^{1.4}. \quad (7)$$

The knowledge of A_v/A_w is also needed to estimate the steam and heater radii. However, to calculate these quantities, we further need the site density information. There are a number of studies where the site density is measured as a function of surface heat flux. However, in almost all those studies, the measurement was only possible at low heat fluxes producing the discrete bubble region. The resulting empirical expressions must be extrapolated to higher heat fluxes with one such expression by Gaertner [1], given by

$$q = 117.1\left(\frac{N}{A_w}\right)^{2/3} \quad (8)$$

where q is in W m^{-2} and N/A_w is in sites m^{-2}. This relationship is used in the present model. Knowing A_v/A_w and N/A_w, we can estimate the stem radius and the corresponding heater radius for an average stem.

Model solution

We nondimensionalize the combined fluid and heater equation set and solve them using the standard explicit finite-difference scheme that employs relaxation for rapid convergence. Further discussion on this subject can be found in our report [11].

RESULTS

Initially, we concentrated on the results of boiling over a thick copper block heated by cartridge heaters. Detailed results from various parametric studies are reported elsewhere [11, 23].

Boiling on a thick copper block

Initially, we compared the model with the small diameter, water-on-copper boiling data of Katto and Yokoya [7]. The advantage of this data set is that it was obtained using a small enough boiling surface that only one mushroom bubble was present on the surface at a time. On the other hand, with the exception of the hovering period, none of the quantities required for closure, such as the initial macrolayer thickness, number density, and surface void fraction was measured in these tests. To simulate their thick copper block, we used a uniform heat-flux boundary condition at the bottom of a 10 mm thick heater. A 10 mm thick block was found to satisfactorily represent an infinitely thick copper block. Table 1 provides the necessary closure parameters derived from the relationships described in the previous section.

The triple-point, mass-evaporation coefficient $m_{e,TP}$ for various fluid–heater surface combinations is currently unknown. We determined this coefficient in an indirect fashion by tuning the computer simulation program to match a single experimental data point of the 1.075 MW m^{-2} heat flux and 16.5°C wall superheat for the average vapor stem. The choice of this data point was arbitrary. This tuning yielded $m_{e,TP} = 6(10^{-5})$ kg m^{-1} s^{-1} °C^{-1}. Subsequently, the same constant was used at all heat-fluxes on the boiling curve. Note that for steady-state conduction to provide this magnitude of evaporation, a thin microlayer underneath the stem with an average thickness of less than 2 μm is required.

Figure 3 shows the individual evaporation contributions of the macrolayer top surface, stem interface, triple-point and resulting instantaneous thinning rate of the macrolayer at the converged hovering period at a heat flux of 1.075 MW m^{-2}. The percentage of macrolayer evaporated is about 25% of complete evaporation. The top surface, stem interface, and triple-point evaporation contributions (relative to total evaporation) are 12, 1 and 87%, respectively. This clearly indicates that the triple-point evaporation effect is the dominant latent heat-transport mechanism. This small evaporative effect from the stem

Table 1. Geometric parameters for current results

q (MW m^{-2})	δ_0 (m)	R_s (mm)	R_h (mm)	A_v/A_w (%)	τ_d (ms)
0.674	0.197	0.114	0.825	1.91	46.1
0.814	0.140	0.101	0.734	1.89	47.9
1.075	0.098	0.085	0.595	2.04	50.6
1.406	0.0655	0.072	0.485	2.20	53.4

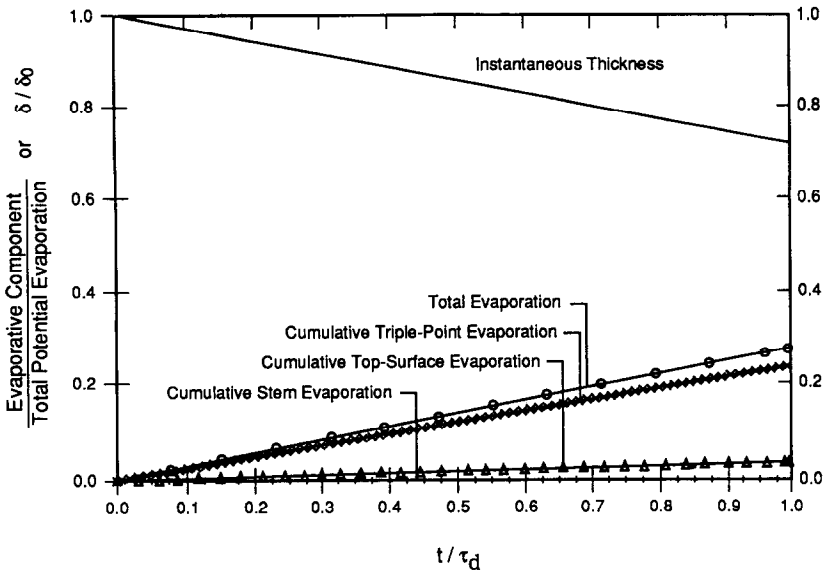

FIG. 3. Relative contributions to macrolayer thinning for $q = 1.075$ MW m^{-2}.

and macrolayer–bubble interfaces is obtained even assuming the maximum possible heat transfer from the macrolayer to the vapor. The boundary conditions for these interfaces are equivalent to assuming an infinite heat-transfer coefficient. The results of the relative evaporation contributions for all heat fluxes studied are shown in Table 2. Triple-point evaporation ranges from a minimum of about 82% to a maximum of 95% over the heat-flux ranges considered.

To further assess the relative influence of the triple-point (microlayer) evaporation, we conducted the following test. At the same heat-flux (1.075 MW m^{-2}) where the triple-point evaporation coefficient was tuned, the triple-point mass-evaporation coefficient was set to zero. The period and surface-averaged wall superheat was found to be about 97°C. This is about six times higher than the observed experimental wall superheat (16.5°C). Transient thermal transport into the macrolayer itself and axial conduction into the stem are totally inefficient in providing the needed cooling. This result indicates that the heater surface must be cooled by the triple-point evaporation mechanism.

To investigate the effect of the surface void ratio on the transient model, we performed the same calculation, $m_{e,TP} = 0$, with a void ratio of 10%, using the same macrolayer thickness. The period- and surface-averaged heater surface superheat was 96.2°C. Increasing the void fraction by a factor of five produces no significant change in the predicted surface superheat. This establishes that, for complete macrolayer resupply and surface void fractions similar to those reported in the literature, stem interface and macrolayer top-surface evaporation and transient storage within the macrolayer cannot cool the surface to the observed superheat.

Another way of obtaining comparably lower surface superheats would be to artificially enhance the thermal conductivity of the liquid within the macrolayer, as recommended by Pan and Lin [18]. Keeping all the closure parameters the same as before, setting $m_{e,TP} = 0$, and using the recommended $k_f = 2.5$ W m^{-1} °C^{-1} (molecular thermal conductivity for saturated water at amospheric pressure is ~0.7 W m^{-1} °C^{-1}), we obtain a surface superheat of 29.9°C for 1.075 MW m^{-2}. This value is still higher than the experimental superheat. To match the experimental data, a larger value for the effective thermal conductivity must be used. However, we think such enhancement is only valid near the vapor stem resulting from high vapor velocities in the stem and Marangoni effects that induce a localized flow within the macrolayer. This effect is already lumped into our triple-point evaporation coefficient. Pan *et al.* [16]

Table 2. Macrolayer evaporation for copper

q_e (MW m^{-2})	Total $\Delta\delta$ (mm)	Triple point (%)	Top surface (%)	Stem (%)
0.674	0.0124	95.4	3.9	0.7
0.814	0.0165	91.7	7.4	0.9
1.075	0.0245	87.5	12.1	0.4
1.406	0.0350	81.8	17.7	0.5

proposed that the surface tension-driven Marangoni flow may be responsible for such enhanced thermal conductivity. The necessary liquid velocities to support this claim must be quite large and cannot be easily justified within the transient phenomenon of interest. We think that further studies are necessary to investigate this claim.

Using a constant value for the triple-point evaporation coefficient, the resulting boiling curve is shown in Fig. 4 along with the data of Katto and Yokoya [7]. As shown, the prediction is reasonable. A surprising result obtained from the model was a curve-back effect where the average surface temperature does not increase at a high enough rate (at the rate the experimental values increase) with increasing heat flux. Actually, the surface temperature decreases when the heat flux is increased from 1.075 to 1.406 MW m^{-2}. While it is possible to improve on the shape of this curve by adjusting $m_{e,TP}$ at each point on the boiling curve, we believe that the triple-point mass-evaporation mechanism is a function of liquid/solid contact angle only and can be left as a constant.

Physically, curve-back might be caused by the fact that, during the hovering period, the liquid layer becomes thin enough that surface evaporation becomes important, resulting in accelerated macrolayer thinning. The nonlinear effect of accelerated thinning might then result in a curve-back effect when a single stem size is considered. On a real heater surface with boiling, where many stems having various macrolayer thickness are available, curve-back might not be experimentally observed. To further examine this possibility, we artificially increased the initial macrolayer thickness, shown in Table 1, by an order of magnitude (we set $\delta_0 = 0.655$ mm) and re-ran the case for $q_e = 1.406$ MW m^{-2}. The resulting average surface superheat is 18.05°C (experimental value is ~18°C). Thus, some nonlinear acceleration of thinning is being observed even for the ~18% evaporation shown in Table 2, and a sensitivity to the initial macrolayer thickness exists at these high test fluxes.

Another potential influence arising from the closure relationships is from the stem spacing, i.e. number density and/or surface void fraction with increasing heat flux. We investigated the sensitivity of the curve-back phenomenon to the number density correlation used. While keeping all other parameters the same, we adjusted the number density until we matched the experimental superheat for $q_e = 1.406$ MW m^{-2}. The resulting number density is 1.0001×10^6 m^{-2}, which is 24% smaller than the magnitude predicted by equation (9). If we recast this number density change into the form of equation (9), while keeping the constant 117.1 the same, we obtain an exponent of 0.68 instead of 0.66. This variation is certainly within the accuracy range of the correlation, especially considering that it has to be extrapolated to higher heat fluxes beyond its original database.

These results indicate that there are still a number of unknowns in high heat-flux nucleate boiling of saturated liquids, and the modeling requires further refinement. We expect the deviation between the model results and the data to be the result of the following weaknesses or inaccuracies in the model:

(1) We know neither the exact number density nor the surface void fraction for the data of Katto and Yokoya [7]. These quantities are expected to be dependent on the contact angle and surface preparation techniques. Unfortunately, the results show strong sensitivity to these closure relationships. Further, the empirical correlations used for these quantities come from relatively large boiling surfaces. For the small boiling surface data of Katto and Yokoya [7], these quantities may be affected by the edge effects and the liquid supply from the vapor mushroom periphery. A similar statement could be made concerning the initial macrolayer thickness.

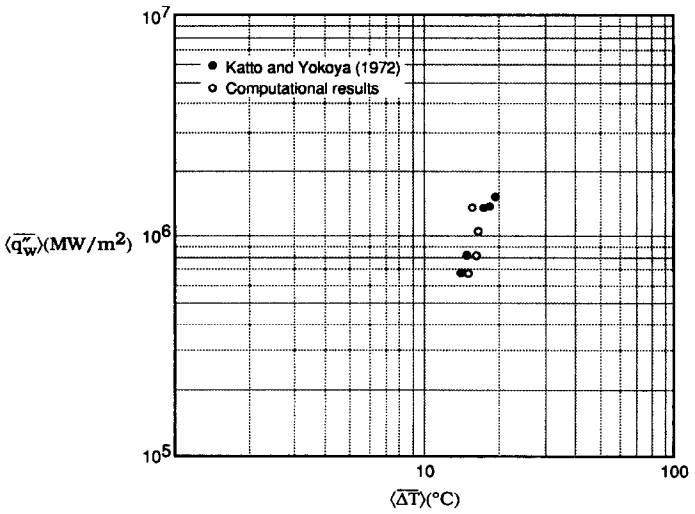

FIG. 4. Comparison of the model prediction with the data of Katto and Yokoya [7].

(2) The triple-point modeling quantified by the evaporation rate is a highly linearized function of the triple-point temperature and the stem radius. If, indeed, this evaporation is related to liquid penetration under the stem (microlayer) and the enhanced conduction due to high vapor velocity in the stem that stirs the liquid near the stem periphery, the relationship is expected to be more nonlinear. Thus, better phenomenological modeling of the triple-point is needed to improve the model.

Effect of heater material and heater thickness

During the course of the present study, we have also investigated the effects [11] of heater material and heater thickness using the current model. Using materials with a smaller thermal conductivity, the boiling curve shifts to the right (lower heat-transfer coefficients), in agreement with most of the available literature. This behavior is associated with the fact that the heat-transfer process is dominated by triple-point evaporation, and the lower thermal conductivity materials have less capability to transport the thermal heat within the solid radially from under the macrolayer toward the triple-point. For the thick copper heater, the radial temperature variations are observed to be relatively small. Typically, the maximum difference is less than 3°C for the heat fluxes and average-stem configurations investigated in this paper. For a nickel heater of the same thickness (10 mm), the maximum radial temperature variation is in excess of 10°C, which results in an increase in the surface-averaged wall superheat for the same heat flux.

For very thin materials with low thermal conductivity (1 μm thick nickel), the maximum radial variation becomes in excess of 100°C. For such high values of local superheats, additional sites must be activated. However, within the current calculations this activation is prevented through the use of equation (8), which specifies the number of active sites. Physically, the activation of additional sites depends on both the distribution of potential sites on the surface and the superheat present at each potential site. And although we cannot currently determine the final superheat for this situation, the model is at least trying to tell us that more active nucleation sites are required. This result indicates that the final wall superheat solution would be controlled by the coupled interaction of the multidimensional wall superheat solution within the heater and heater–surface effects, including cavity distribution, site activation, and triple-point characteristics including contact angle.

SUMMARY AND CONCLUSIONS

In this study, we analyzed the high heat-flux, nucleate boiling phenomenon. We developed a new model, which is based also on the macrolayer approach. The novelty of this model is in its capability of looking at the problem from a transient 2D point of view.

We coupled and solved the conduction equation within the heater and liquid macrolayer. During the bubble growth, the macrolayer becomes thinner due to evaporation and is modeled as uniform in the radial direction. The model requires a number of closure relationships. These relationships for the initial macrolayer thickness, number density, and wall void fraction are obtained from empirical models or data that are available in the literature. There is no single study where all of these parameters have been measured within a given experimental setup. Thus, we had to mix and match. All empirical information was obtained from experimental studies where saturated water at amospheric pressure was boiled on a copper heater. However, the surface preparation techniques are likely to be different for these experiments.

Thus, not only is the final model restricted to boiling of saturated water at atmospheric pressure over a copper heater, it is also further restricted, within this definition, by the unknown accuracy in extrapolating the closure relationships from one experiment to another. Nevertheless, we believe the present study provided some valuable information. While the quantitative implications of these observations must be used with care, the qualitative implications are quite informative and can be itemized as follows:

(1) While experimental evidence indicates the existence of a thin macrolayer under a growing bubble, transient conduction within this layer cannot be solely responsible for the high heat-transfer rates observed in nucleate boiling. Evaporation at the macrolayer's upper and stem interfaces are not significant, contrary to the findings of a number of previous investigators. Inherent within this result is the effect of liquid resupply of the macrolayer at bubble departure and what happens to the thermal boundary layer at the time of resupply. Yu and Mesler [5] indicate an answer to this question, but we believe the question is so important that confirmatory work is required.

(2) Most of the evaporation has to occur under the stem or near the stem periphery to match the boiling curve data. Quantitatively, this observation is in agreement with the existence of a microlayer under a stem [15]. If this mechanism dominates, one would expect the radius must either grow or liquid must flow to replenish the microlayer.

(3) We have a highly linearized empirical model for triple-point evaporation. Currently, we associate the high evaporation rate at this point with (1) the formation of a microlayer, and (2) enhanced thermal evaporation near the vapor stem as a result of the high vapor velocities in the stem and the potential for Marangoni flow in this immediate microlayer region. Also, the scale may well be small enough that molecular forces come into effect. Further research is required for phenomenological modeling of this quantity.

(4) Using the current closure relationships, we observe a curve-back effect (ΔT_w decreases with

increasing heat flux) at heat fluxes near CHF. One cause of this behavior is the use of a single 'average' stem and the nonlinear thinning effect. Local macrolayer thickness is probably a function of location on the boiling surface and not uniform due to the liquid resupply mechanism after bubble departure. Also, consideration of multiple stems with different radii minimize this effect [24]. The other cause of curveback is a strong sensitivity to the closure relationships, in particular the active-site number density.

(5) The question of surface preparation effects and contact angle effects on the closure relationships, which was not addressed in this study, are important. The contact angle is effectively included within the definition of the triple-point evaporation coefficient.

(6) For thick high thermal conductivity heaters such as copper, the temperature gradient in the radial direction is small, in the order of 3°C. Materials having a lower conductivity show increasing averaged wall temperatures, on the order of 10°C radial variation. Thin nonisothermal materials and thinner isothermal materials show further increases in the superheat under the macrolayer away from the triple point. These superheats are so high that additional nucleation sites must be activated.

REFERENCES

1. R. F. Gaertner, Photographic study of nucleate pool boiling on a horizontal surface, *Trans. ASME J. Heat Transfer* **87,** 17–79 (1965).
2. Y. Iida and K. Kobayasi, Distribution of void fraction above a horizontal heating surface in pool boiling, *Bull. JSME* **12,** 283–290 (1969).
3. A. M. Bhat, J. S. Saini and R. Prakash, Role of macrolayer evaporation in pool boiling at high heat flux, *Int. J. Heat Mass Transfer* **29,** 1953–1961 (1986).
4. S. P. Liaw and V. K. Dhir, Void fraction measurements during saturated pool boiling of water on partially wetted vertical surfaces, *Trans. ASME, J. Heat Transfer* **111,** 731–738 (1989).
5. C.-L. Yu and R. B. Mesler, A study of nucleate boiling near the peak heat flux through measurements of transient surface temperature, *Int. J. Heat Mass Transfer* **20,** 827–840 (1977).
6. Y. Katto and S. Yokoya, Principle mechanisms of boiling crisis in pool boiling, *Int. J. Heat Mass Transfer* **11,** 993–1002 (1968).
7. Y. Katto and S. Yokoya, Behavior of vapor mass in saturated nucleate and transition boiling, *Heat Transfer—Jap. Res.* **5,** 45–65 (1976).
8. Y. Haramura and Y. Katto, A new hydrodynamic model of critical heat flux, applicable widely to both pool and forced convection boiling on submerged bodies in saturated liquids, *Int. J. Heat Mass Transfer* **26,** 389–399 (1983).
9. K. Okuyama, Y. Kozawa, I. Inoue and S. Aoki, Transient boiling heat transfer characteristics of R113 at large stepwise power generation, *Int. J. Heat Mass Transfer* **31,** 2161–2174 (1988).
10. K. O. Pasamehmetoglu, R. A. Nelson and F. S. Gunnerson, Critical heat flux modeling in pool boiling for steady-state and power transients, *Trans. ASME, J. Heat Transfer* **112,** 1048–1057 (1990).
11. K. O. Pasamehmetoglu, P. R. Chappidi and R. A. Nelson, Pool boiling mechanisms in saturated liquids at high heat fluxes near critical heat flux, Los Alamos National Laboratory report LA-UR-92-935 (1992).
12. A. M. Bhat, R. Prakash and J. S. Saini, On the mechanism of macrolayer formation in nucleate pool boiling at high heat fluxes, *Int. J. Heat Mass Transfer* **26,**735–740 (1983).
13. A. M. Bhat, R. Prakash and J. S. Saini, Heat transfer in nucleate pool boiling at high heat fluxes, *Int. J. Heat Mass Transfer* **26,** 833–840 (1983).
14. A. M. Jairajpuri and J. S. Saini, A new model for heat flow through macrolayer in pool boiling at high heat fluxes, *Int. J. Heat Mass Transfer* **34,** 1579–1591 (1991).
15. M.-C. Chyu, Evaporation of macrolayer in nucleate boiling near burnout, *Int. J. Heat Mass Transfer* **30,** 1531–1538 (1987).
16. C. Pan, J. Y. Hwang and T. L. Lin, The mechanism of heat transfer in transition boiling, *Int. J. Heat Mass Transfer* **32,** 1337–1349 (1989).
17. V. K. Dhir and S. P. Liaw, Framework for a unified model for nucleate and transition pool boiling, *Trans. ASME, J. Heat Transfer* **111,** 739–746 (1989).
18. C. Pan and T. L. Lin, Marangoni flow on pool boiling near critical heat flux, *Int. Commun. Heat Mass Transfer* **16,** 475–486 (1989).
19. D. B. Kirby and J. W. Westwater, Bubble and vapor behavior on a heated horizontal plate during pool boiling near burnout, *Chem. Engng Prog. Symp. Ser.* **61,** 57 (1965).
20. H. J. Van Ouwerkerk, Burnout in pool boiling the stability of boiling mechanism, *Int. J. Heat Mass Transfer* **29,** 25–34 (1972).
21. K. O. Pasamehmetoglu, R. A. Nelson and F. S. Gunnerson, Study of the hovering period and bubble size in fully developed pool nucleate boiling of saturated liquid with a time-dependent heat source, *Nonequilibrium Transport Phenomena*, ASME HTD-Vol. 77, pp. 39–45. ASME, New York (1987).
22. K. O. Pasamehmetoglu and R. A. Nelson, The effect of Helmholtz instability on the macrolayer thickness in vapor mushroom region of nucleate pool boiling, *Int. Commun. Heat Mass Transfer* **14,** 709–720 (1987).
23. P. R. Chappidi, C. Unal, K. O. Pasamehmetoglu and R. A. Nelson, Development of multiple-vapor-stem model for saturated pool nucleate boiling at high heat fluxes on a horizontal surface, Los Alamos National Laboratory report, LA-UR-91-1939 (1991).
24. P. R. Chappidi, C. Unal, K. O. Pasamehmetoglu and R. A. Nelson, Statistical consideration of vapor stem radii for the analysis of saturated pool nucleate boiling at high heat fluxes in vapor mushroom region, *Phase Change Heat Transfer-1991*, ASME HTD-Vol. 159, pp. 119–130 (1991).